

pubs.acs.org/journal/apchd5 Article

Temporal Coupled Mode Analysis of Chromaticity in Trilayer Subtractive Structural Colors

Wei-Jie Feng, Yian Cheng, and L. Jay Guo*



Cite This: ACS Photonics 2023, 10, 2784–2792



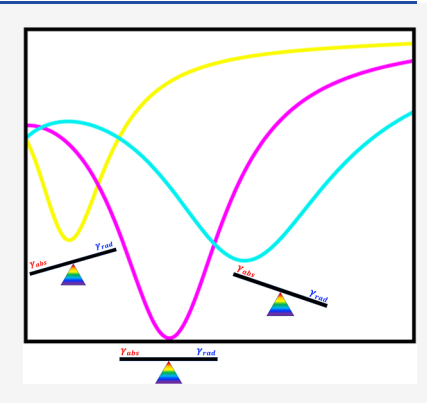
ACCESS I

III Metrics & More

Article Recommendations

Supporting Information

ABSTRACT: We present a new way of understanding the spectral behavior of a Fabry—Perot-type trilayer stack for a subtractive structural color based on a temporal coupled mode analysis. This cavity-based analysis is able to fit reflection spectra feature and predict color chromaticity well even without taking material dispersion into account. To produce the most chromatic color, this analysis reveals that matching of absorptive and radiative decay rates while both being maximized is the key, which leads to a broad and highest absorption peak. Inclusion of an ultrathin high-index dielectric on top of the lossy bottom layer can further boost the absorptive decay rate of the cavity, which helps to fine-tune color chroma. Both simulation and experimental results are presented in accordance with color chromaticity predicted by the temporal coupled mode analysis.



KEYWORDS: structural color, chromaticity, temporal coupled mode theory

INTRODUCTION

Chroma, one of the three dimensions (lightness, hue, and chroma) for color representation, is a unique parameter for perceiving the degree of color saturation. In the past decade, structural color designed from stratified layers²⁻⁴ has proven to be one of the most promising ways to achieve industrial level production due to its simple structure as well as numerous coating methods available. These layered structural color pigments offer advantages such as long-term durability, brilliant coloration, environmental friendliness, and providing special visual effects (e.g., iridescence). Several previous attempts have been made to create high chromatic colors with various strategies. 5-7 Among them, a Fabry-Perot-type trilayer stack turns out to be the simplest but effective way of producing a large variety of colors. However, a mechanism study on such Fabry-Perot-type structural color chromaticity is still lacking, apart from using numerical optimization methods to fine-tune the layered structures. The colors seen from the trilayer structure are typically associated with the optical resonance phenomenon in such an optical cavity where a resonance dip is usually observed in the reflection spectrum, giving subtractive primaries like yellow, magenta, and cyan colors. Typical spectral behaviors are illustrated in Figure 1, where three different scenarios are compared to get a general idea of the spectra-chromaticity relation.

The first scenario refers to the two spectra with exactly the same resonance dip but different background reflections (Figure 1a), where the corresponding CIEL*a*b* coordinates indicate that a higher chromaticity is achieved with a lower background reflection (Figure 1d). In the second scenario, two

spectra with the same level of background reflection are presented but with a difference in their reflection minimum (Figure 1b). The corresponding chromaticity diagram then favors the spectra with a lower reflection minimum (Figure 1e). The last scenario, where both spectra have the same reflection minimum but different in dip width (Figure 1c), reveals a higher chromaticity with a further broadening of the dip (Figure 1f). One could then come up a rough idea that a high chromatic color usually requires a low minimum reflection on resonance as well as a certain broadening of the dip.8-10 Though a few works have demonstrated very high chroma colors with design principles for each layer, a high-level understanding between the layer cavity behavior and its chromaticity performance is still lacking. To address this longstanding problem, we adopt a temporal couple mode (TCM) analysis 11,12 to describe such a trilayer system with two energy decay channels for absorption and radiation. While transfer matrix method (TMM) calculation requires exact material dispersion, temporal coupled mode theory (TCMT) does not. However, the two methods provide a fairly good match as shown in (Figure 2), especially in the vicinity of the resonance wavelength. The spectral feature and the resulting color

Received: April 12, 2023 Published: July 6, 2023





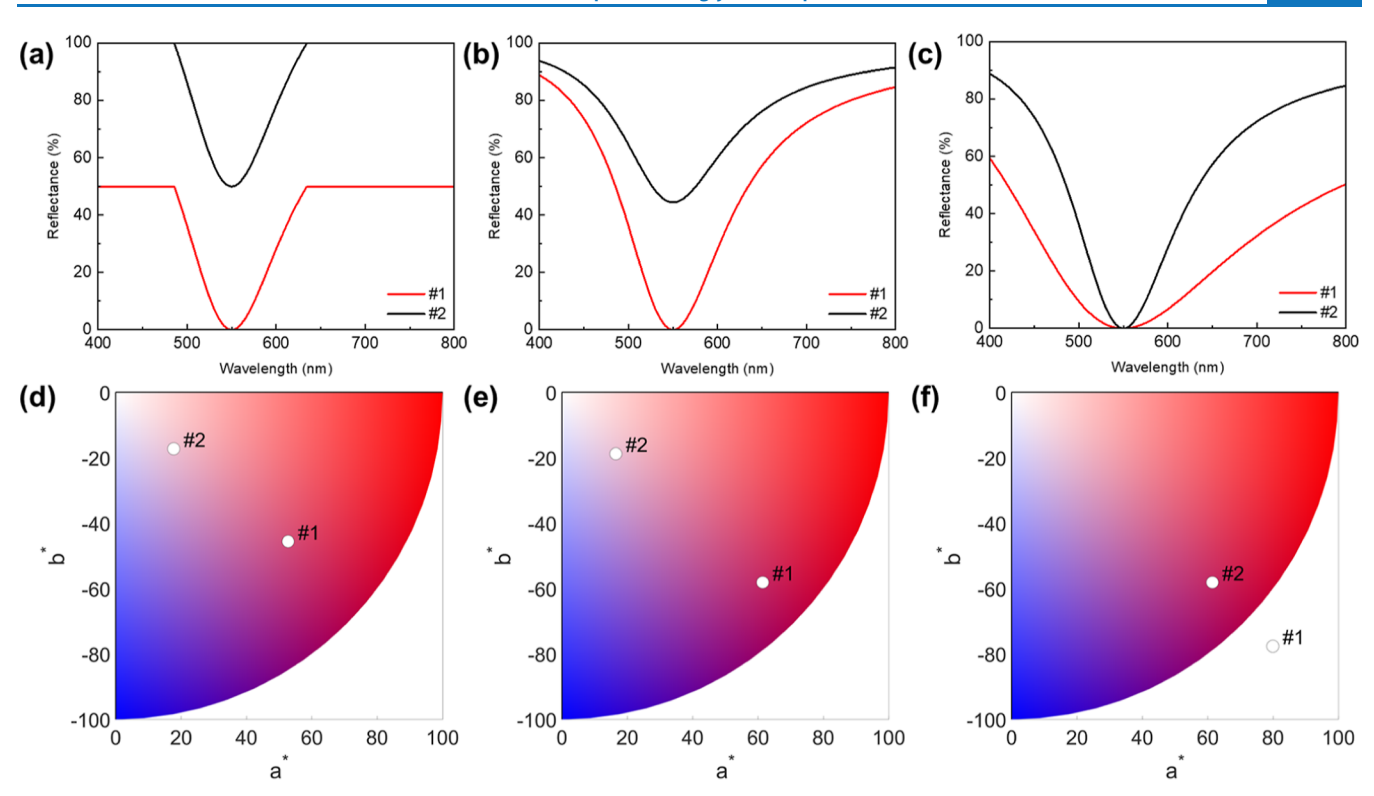


Figure 1. (a-c) Three scenarios for a typical trilayer subtractive color with a dip in the reflection spectra and (d-f) their corresponding CIEL*a*b* coordinates. Points further away from the center represent higher color chroma. All CIEL*a*b* color coordinates are calculated in reference to a standard D65 illuminant.

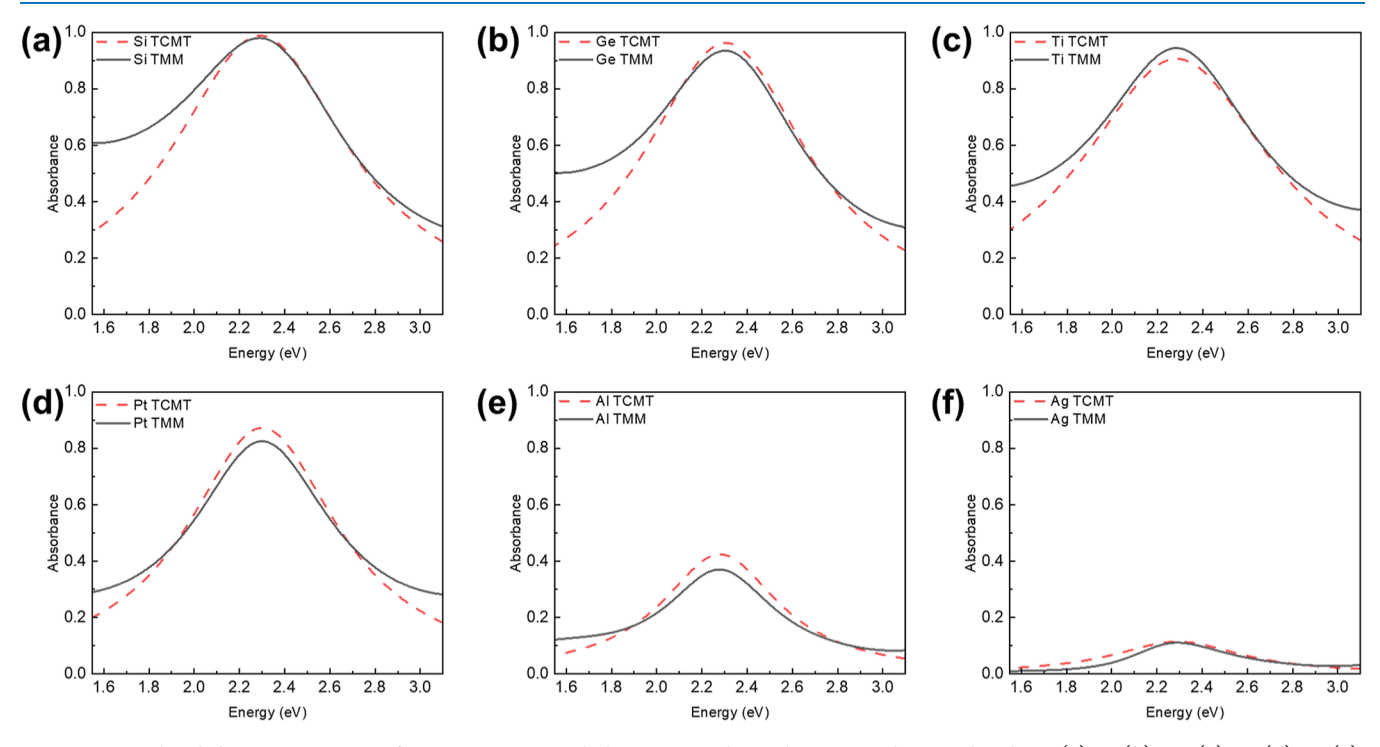


Figure 2. Simulated absorption spectra of HLA structures in dark magenta color with various substrate absorbers: (a) Si, (b) Ge, (c) Ti, (d) Pt, (e), Al, and (f) Ag. A close match between the two simulation methods TMM (solid line) and TCMT (dash line) in the vicinity of the absorption peak is observed.

chroma can be fully captured competing between the two decay rates. A high chromatic color is realized only if decay rates are large and well balanced simultaneously, which fully coincides with the observation shown in Figure 1. Hence,

instead of a wavelength-by-wavelength calculation, a resonance wavelength-based analysis is capable of predicting the chromaticity performance for the trilayer subtractive structural color.

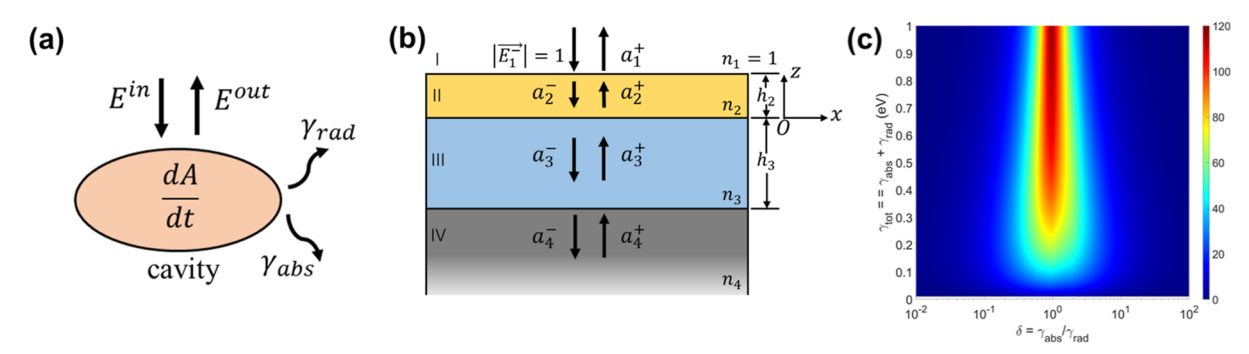


Figure 3. (a) Schematic model for a single-port resonator. (b) Trilayer stack with the incident electric field amplitude normalized to 1 V/m (in air). (c) Color chroma represented in color map calculated from eq 2 by varying two decay rates γ_{abs} and γ_{rad} with an increment of chromaticity from blue to red.

METHODS

A typical analysis for multilayer structural color usually starts with the multilayer interference model,¹³ followed by a phase analysis for each layer to determine the resonance feature of the resulting spectra or color appearance. ^{9,10,14–19} A perfect absorption at the designed wavelength is reached if the multilayer reflection wave cancels the direct reflection at the first interface in both phase and amplitude. 20-22 However, since the multilayer interference formalism calculates the reflection layer by layer, limited information can be extracted to understand the effect of material optical properties has on the entire stack as well as its color performance. To address this problem, we introduce another way of understanding the multilayer structural color based on cavity analysis. More specifically, we focus on a rather simple but effective trilayer structure² (e.g., metal/dielectric/metal) that can produce a wide range of colors from yellow, magenta to cyan. The trilayer structure forms a simple Fabry-Perot (F-P) cavity, with the resonance mode being defined by the thickness of the cavity. With the light incident onto the multilayer resonator surface, part of the energy is directly reflected from the top surface and the rest couples into the cavity. By using a sufficiently thick and absorbing bottom layer, the resonance energy leaks out in the same direction as the direct reflection; hence, a single-port model can be used.

The TCMT is established based on the time-dependent formalism of an optical resonator. As stated above, we consider a single-mode optical resonator with only a single port coupled to the environment. Such a model can be used to completely describe a simple trilayer structure with only a reflection port at resonance condition. As illustrated in Figure 3a, the dynamics of the field amplitude A inside the resonator can be described as follows

$$\begin{cases} \frac{\mathrm{d}A}{\mathrm{d}t} = (-i\omega_0 - \gamma_{\mathrm{abs}} - \gamma_{\mathrm{rad}})A + c_{\mathrm{in}}E^{\mathrm{in}} \\ E^{\mathrm{out}} = c_{\mathrm{bkg}}E^{\mathrm{in}} + c_{\mathrm{out}}A \end{cases}$$
(1)

where ω_0 is the resonant frequency, $c_{\rm in}$ is the coupling coefficient between the resonance and incoming wave, $\gamma_{\rm abs}$ and $\gamma_{\rm rad}$ are the decay rates of the resonance due to intrinsic resonator absorption and external leakage, respectively, $c_{\rm bkg}$ is the background reflection coefficient directly connecting the incoming and outgoing waves, which only adds a phase ϕ to the incoming wave if the cavity is lossless, and $c_{\rm out}$ is the coupling coefficient between the resonance and the outgoing wave. Considering the law of energy conservation as well as

time-reversal symmetry, 23 we can find that $c_{\rm in}=c_{\rm out}=\sqrt{2\gamma_{\rm rad}}e^{i(\frac{\phi}{2}+\frac{\pi}{2}+N\pi)}$ with N to be an arbitrary integer. We can then further solve eq 1 for the reflection coefficient as

$$r = \frac{E^{\text{out}}}{E^{\text{in}}} = e^{i\phi} + \frac{2e^{i\phi}\gamma_{\text{rad}}}{-i(\omega - \omega_0) + \gamma_{\text{rad}} + \gamma_{\text{abs}}}$$
(2)

and absorption can be calculated as

abs = 1 -
$$r^*r = \frac{4\gamma_{rad}\gamma_{abs}}{(\omega - \omega_0)^2 + (\gamma_{rad} + \gamma_{abs})^2}$$
 (3)

Therefore, a perfect absorption (i.e., unity absorption) can be achieved at resonance $(\omega-\omega_0)$ only when $\gamma_{abs}=\gamma_{rad}$, which is typically referred to as the critical coupling condition. Meanwhile, we can also obtain the absorptive and radiative quality factors, respectively, as

$$Q_{abs} = \frac{\omega_0 U}{P_{abs}} = \frac{\omega_0}{2 \gamma_{abs}}, \qquad Q_{rad} = \frac{\omega_0 U}{P_{rad}} = \frac{\omega_0}{2 \gamma_{rad}}$$
(4)

with U as the energy stored inside the cavity and P_{diss} and P_{abs} represent the dissipation power due to absorption and radiation, respectively. Note that the features of the reflection spectrum are strongly related to the overall decay rate $\gamma_{\rm tot} = \gamma_{\rm abs} + \gamma_{\rm rad}$, which determines the broadening/width of the resonance in the spectrum and the ratio $\delta = \gamma_{\rm abs}/\gamma_{\rm rad}$ determines the minimum reflectance at resonance wavelength. When $\delta = 1$, the reflection dip can reach zero, corresponding to the critical coupling condition. We define chromaticity as $C = \sqrt{a^{*2} + b^{*2}}$, where a^* and b^* are the coordinates in the CIEL*a*b* diagram, characterizing the hue level along the red-green and yellow-blue directions. Figure 3c illustrates C as a function of δ and γ_{tot} at different resonance wavelengths, where the red region indicates a high color chroma and the blue region indicates the opposite. The high color chroma region is clearly identified in the vertical central region when the two decay rates are matched, and the highest chroma is achieved toward the top of the red region when both decay rates are maximized. Though the chromaticity varies greatly over different resonance wavelengths due to the correlation between lightness and chroma, they share the same spectrum features in achieving high chroma color. Hence, it gives us a simple yet general design principle to achieve high chroma in single-cavity-based structural colors.

Compared with the multilayer interference theory, TCMT treats the entire structure as a whole and focuses more on the

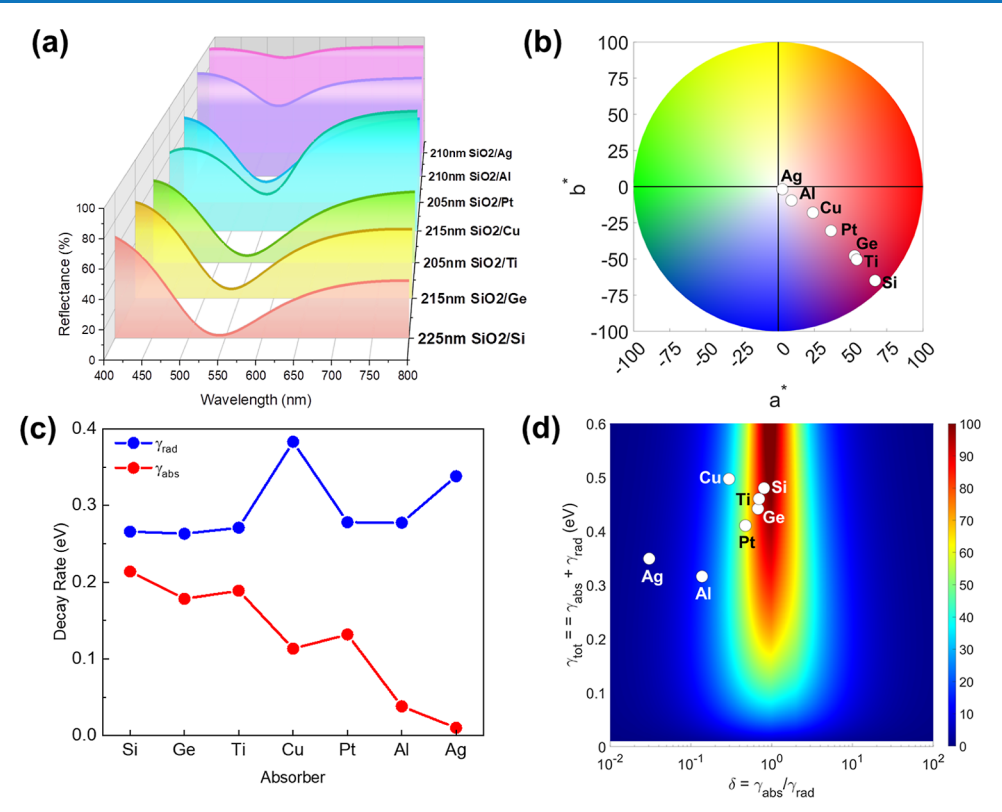


Figure 4. (a) Reflection spectra of 25 nm $TiO_2/SiO_2/absorber$ calculated from TMM for dark magenta color. (b) CIEL*a*b* coordinates calculated from (a). (c) Decay rates extracted using TCMT for 25 nm $TiO_2/SiO_2/absorber$ structure. (d) Color chroma calculated based on the extracted decay rates in (c).

material effects on cavity behavior. Factors affecting the resonance can be more intuitively understood by phenomenological parameters, i.e., the influence of material optical properties on the absorption feature can be characterized with the extraction of the two resonance decay channel rates responsible for absorption and radiation, respectively. 26,27 As a model system, the extraction of the two decay rates of a trilayer structure (Figure 3b) is derived in the following based on Maxwell's equations, assuming a plane wave incident at a normal angle with no transverse mode being excited inside the cavity (i.e., $h_3 \gg 0$); the electromagnetic fields in each layer can be determined from the boundary conditions at each interface (i.e., continuity of tangential E-field and H-field across the interface). The reflection coefficient can then be calculated based on the Fresnel equation, where both real and imaginary parts of the refractive index plays an important role. Take the lossless-lossy material interface with refractive indices n_0 and $n - i\kappa$, the reflectivity can be expressed as

$$R = \frac{\left(\frac{n_0}{n} - 1\right)^2 + \left(\frac{\kappa}{n}\right)^2}{\left(\frac{n_0}{n} + 1\right)^2 + \left(\frac{\kappa}{n}\right)^2} \tag{5}$$

Several conclusions can be drawn from eq 5: (1) a minimum reflectivity can be achieved only when the lossless refractive index squared matches the sum of the real and imaginary parts of the lossy material squared (i.e., $n_0^2 = n^2 + \kappa^2$). (2) A significant amount of reflection can be generated when either $\frac{\kappa}{n}$ is very large or $n \gg n_0$, $\kappa \to 0$. A close to unity reflection could be achieved once $\frac{\kappa}{n} \to +\infty$. This explains why silver, though having a very larger imaginary part accounting for absorption

(Figure S1b), still has an ultrahigh reflectivity across the entire visible range, and copper or gold has very high reflectivity at longer wavelengths.

We can thus expand the electric and magnetic fields in layer i as $E_i = a_i^+ e^{ik_iz} + a_i^- e^{-ik_iz}$ and $H_i = \frac{n_i}{Z_0} (a_i^+ e^{ik_iz} - a_i^- e^{-ik_iz})$ $E_i = a_i^+ e^{ik_iz}$, with k_i being the wavevector, and the boundary conditions at three interfaces $(z = -h_2, 0, and h_3)$ are written as

$$\begin{cases} a_{1}^{+}e^{ik_{1}h_{2}} + e^{-ik_{1}h_{2}} = a_{2}^{+}e^{ik_{2}h_{2}} + a_{2}^{-}e^{-ik_{2}h_{2}} \\ \frac{1}{Z_{0}} \left(a e^{ik_{1}h_{2}} - e^{-ik_{1}h_{2}} \right) = \frac{n_{2}}{Z_{0}} \left(a e^{ik_{2}h_{2}} - a_{2}^{-}e^{-ik_{2}h_{2}} \right) \\ a_{2}^{+} + a_{2}^{-} = a_{3}^{+} + a_{3}^{-} \\ \frac{n_{2}}{Z_{0}} \left(a - a_{2}^{-} \right) = \frac{n_{3}}{Z_{0}} \left(a - a_{3}^{-} \right) \\ a_{3}^{+}e^{-ik_{3}h_{3}} + a_{3}^{-}e^{ik_{3}h_{3}} = a_{4}^{-}e^{ik_{4}h_{3}} \\ \frac{n_{3}}{Z_{0}} \left(a - e^{-ik_{3}h_{3}} - a_{3}^{-}e^{ik_{3}h_{3}} \right) = -\frac{n_{4}}{Z_{0}} \left(a - e^{ik_{4}h_{3}} \right) \end{cases}$$

$$(6)$$

where all fields are normalized with respect to the incident field $E_1^-(z \ge h_2) = 1$ and Z_0 represents the vacuum impedance. By solving the electric field from eq 6, we can further extract time-averaged energy stored inside the cavity $U = U_{E_3} + U_{H_3}$ as

$$\begin{cases} U_{E_3} = \frac{1}{2} Re \left\{ \varepsilon_0 \varepsilon_3 \int_{-h_3}^0 E_3^* E_3 \, \mathrm{d}z \right\} \\ U_{H_3} = \frac{1}{2} Re \left\{ \varepsilon_0 \varepsilon_3 \int_{-h_3}^0 H_3^* H_3 \, \mathrm{d}z \right\} \end{cases}$$

$$(7)$$

where ε_0 is the vacuum permittivity.

Absorptive dissipation power can be derived from the absorption decay channel. Since both the top and bottom layers (layer 2 and layer 4) may absorb light, the total dissipated power from absorption is the sum of these two layers $P_{\rm abs} = P_{\rm 2,abs} + P_{\rm 4,abs}$ and

$$\begin{cases} P_{2,abs} = \frac{1}{2} \text{Im} \{ \varepsilon_0 \varepsilon_2 \} \int_0^{h_2} E_2^* E_2 \, dz \} \\ P_{4,abs} = \frac{1}{2} \text{Im} \{ \varepsilon_0 \varepsilon_4 \} \int_0^{-h_3} E_4^* E_4 \, dz \} \end{cases}$$
(8)

Hence, the absorptive decay rate γ_{abs} can be calculated based on eq 4. Next, we evaluate the power dissipated through radiation loss from the cavity. Note that the total reflected power from the cavity contains both the background reflection directly from the incoming wave and the power coupled out of the cavity (eq 1). Therefore, in order to evaluate the power dissipated purely from the cavity, a pure phase term $e^{i\phi}$ upon background reflection should be taken away from the outgoing wave

$$P_{\text{rad}} = \frac{1}{2} |a_1^+ - e^{i\phi}|^2 \operatorname{Re} \left\{ \oint \overrightarrow{E_1^{*-}} \times \overrightarrow{H_1} \, d\vec{S} \right\}$$
(9)

As a result, the radiative decay rate $\gamma_{\rm rad}$ can be calculated based on eq 4. Hence, both absorptive decay rate and radiative decay rate can be extracted from a trilayer cavity, providing us a new insight for understanding its color performance from a cavity-based point of view.

RESULTS AND DISCUSSION

Chromaticity of the Trilayer HLA Structural Color. We apply the above analysis to a simple trilayer structure consisting of a high-index/low-index/absorber (HLA) and verify our analysis with experimental results. In the HLA structure, the absorptive loss only comes from the bottom absorber. The electric field is confined within the middle low refractive index layer due to the index contrast among the three layers that causes high reflection from the two outmost layers. Therefore, such a trilayer structure can be considered a special, highly asymmetric Fabry-Perot cavity. Though there is no specific requirement in the thickness of each layer (except the bottom layer, which needs to be sufficiently thick to block any transmission), we keep the top high refractive index layer to be thin so that there is negligible resonance inside and our singlecavity analysis applies. The TCMT analysis is then applied to understand how the bottom absorber properties affect the overall color performance of the structure.

Herein, we choose TiO₂ and SiO₂ as the high-index and low-index layers due to their easy accessibility and very-well-developed coating techniques. Four different hues (Figures 4a and S3–S4), namely, yellow, magenta, dark magenta, and cyan, are chosen as examples to evaluate the color performance of the HLA structure as well as the effect of absorbers. Several absorbing materials with very different optical properties are

chosen to provide experimental demonstrations of the two types of decay rates on the color chroma. The materials include silicon (Si), germanium (Ge), titanium (Ti), platinum (Pt), aluminum (Al), silver (Ag), copper (Cu), and gold (Au). As shown in Figure S2, these absorbers have different degrees of light reflection in order to vary the radiative decay rates: silver reflects almost all light across the visible range, silicon reflects only 30% of the spectrum, and copper/gold reflects different wavelength bands due to their absorption from interband transition.²⁵ In order to effectively compare the color performance of various absorbing materials in the 25 nm TiO₂/SiO₂/absorber, the thickness of the middle dielectric layer (SiO₂) is carefully tuned due to the nontrivial phase upon light reflection from the interface of SiO₂/absorber to ensure that all structures give the same hue. The top TiO2 thickness is fixed to be 25 nm, offering a large refractive index contrast but avoiding any resonance mode within the layer.

Chromaticity is then calculated for each sample according to the simulated reflection spectrum from the TMM with all material refractive index being extracted from experiments (Figure S1). Figure 4a,b gives an overview of the HLA color performance in the CIEL*a*b* diagram with the SiO₂ layer thicknesses being carefully tuned to ensure a similar dark magenta hue for different absorber substrates (with resonance dip at ~540 nm, Figure 4a). The trilayer stack with Si as the absorbing substrates give the best chromaticity, followed by Ge or Ti and then Pt, Cu, Al, and Ag (Figure 4b).

TCM analysis is being implemented to reveal the above difference where the deterioration in color chroma is a result of the unbalanced rate between two decay channels (Figure 4c), i.e., $\gamma_{\rm abs}$ and $\gamma_{\rm rad}$ being the absorption loss from the SiO₂/ absorber interface and the radiative loss leaving the cavity, respectively. With a very similar structure, where only the bottom substrate is responsible for absorption, the radiative loss $\gamma_{\rm rad}$ remains high and about the same for structures (except for a jump in Cu is observed in Figure 4c near 540 nm). On the contrary, a huge difference in absorption loss $\gamma_{\rm abs}$ among different absorbers are observed. It turns out that Si has the largest absorption loss to match the radiative loss, followed by Ti, Ge, Pt, Cu, Al, and Ag. Therefore, the best chromaticity is achieved with Si, followed by the order observed in Figure 4b.

As illustrated in Figure 3c, the chroma of a color with a Lorentzian line shape absorption depends on the relative ratio δ between $\gamma_{\rm abs}$ and $\gamma_{\rm rad}$ as well as their sum $\gamma_{\rm tot}$. Hence, we can predict the chromaticity of the aforementioned HLA structural color based on the extract δ and $\gamma_{\rm tot}$ values. As shown in Figure 4d, the predicted color chroma matches very well with the ones from the TMM calculation (Figure 4b), considering that dispersion is being excluded in the TCM calculation, which validates the proposed model. Even colored metals like Cu and Au show a reasonable match in most of the situations, except where the inherent absorption becomes too strong for the TCMT to catch the broadening of the spectrum (e.g., Cu for magenta color). The validity of TCM analysis can be further justified by comparing the absorption spectra (Figures 2 and S7) derived from TMM and TCM. Though a Lorentzian line shape with no material dispersion is being assumed in the derivation of TCM, the absorption spectra match fairly well with those obtained by TMM where the absorbance is rigorously calculated at each frequency, especially near the vicinity of resonance. We attribute such coincidence to the Lorentzian line shape nature of the Fabry-Perot cavity with little dispersion near the resonance wavelength. The TCM

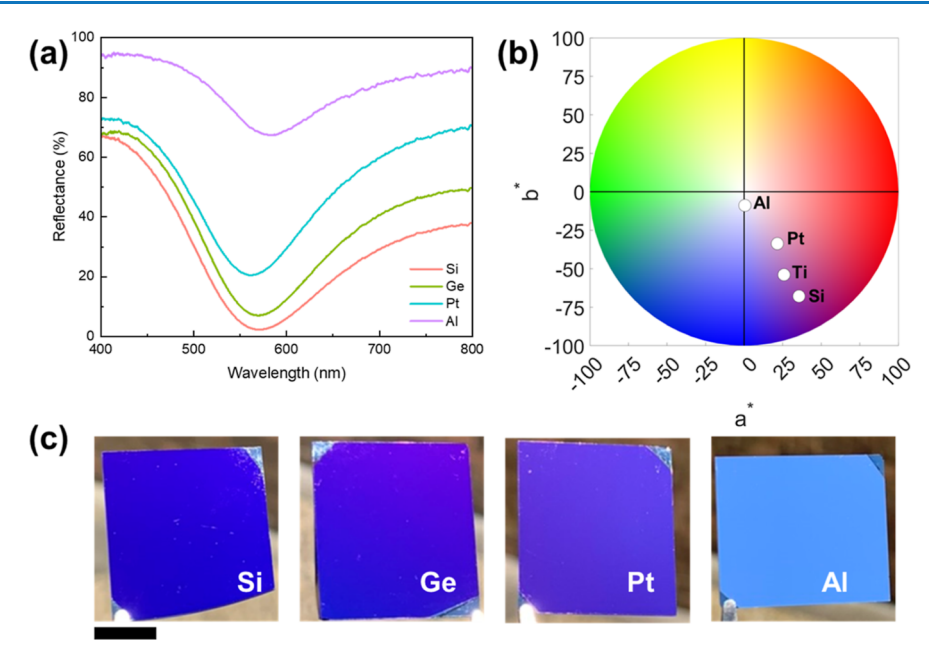


Figure 5. (a) Recorded reflection spectra of fabricated 25 nm $TiO_2/SiO_2/absorber$ and (b) their corresponding CIEL*a*b* coordinates. (c) Photos of the colored samples in (a) taken under direct sunlight illumination. Scale bar: 1 cm.

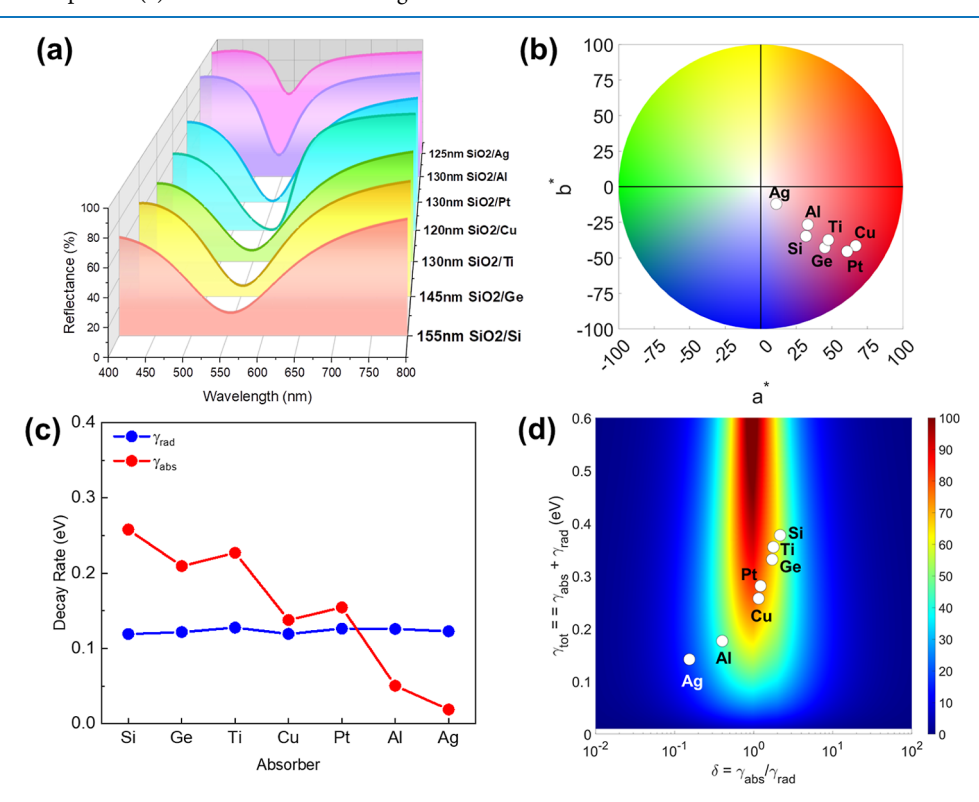


Figure 6. (a) Reflection spectra of 15 nm $Ag/SiO_2/absorber$ calculated from TMM for dark magenta color. (b) CIEL*a*b* coordinates calculated from (a). (c) Decay rates extracted using TCMT for the 15 nm $Ag/SiO_2/absorber$ structure. (d) Color chroma calculated based on the extracted decay rates in (c).

spectra start to deviate from the TMM spectra when the frequency is going farther away from the resonant frequency where strong dispersion comes into play. However, we notice that the TCM-calculated spectrum catches most of the features near resonance except for the amount of background absorption which only affects the lightness of the color rather than chroma. Similar trends are also observed with other colors in yellow, magenta, and cyan by changing the SiO₂ layer

thickness (Figures S3–S6, note that gold is not capable of showing any magenta or cyan-like color due to its strong absorption in the short wavelength).

Experimental realization of the HLA structure is carried out to support the aforementioned material—spectra—color relationship based on TCM analysis. As shown in Figure 5, five HLA samples are fabricated using e-beam evaporation with Al, Pt, Ge, and Si as substrate absorbers. A huge chroma

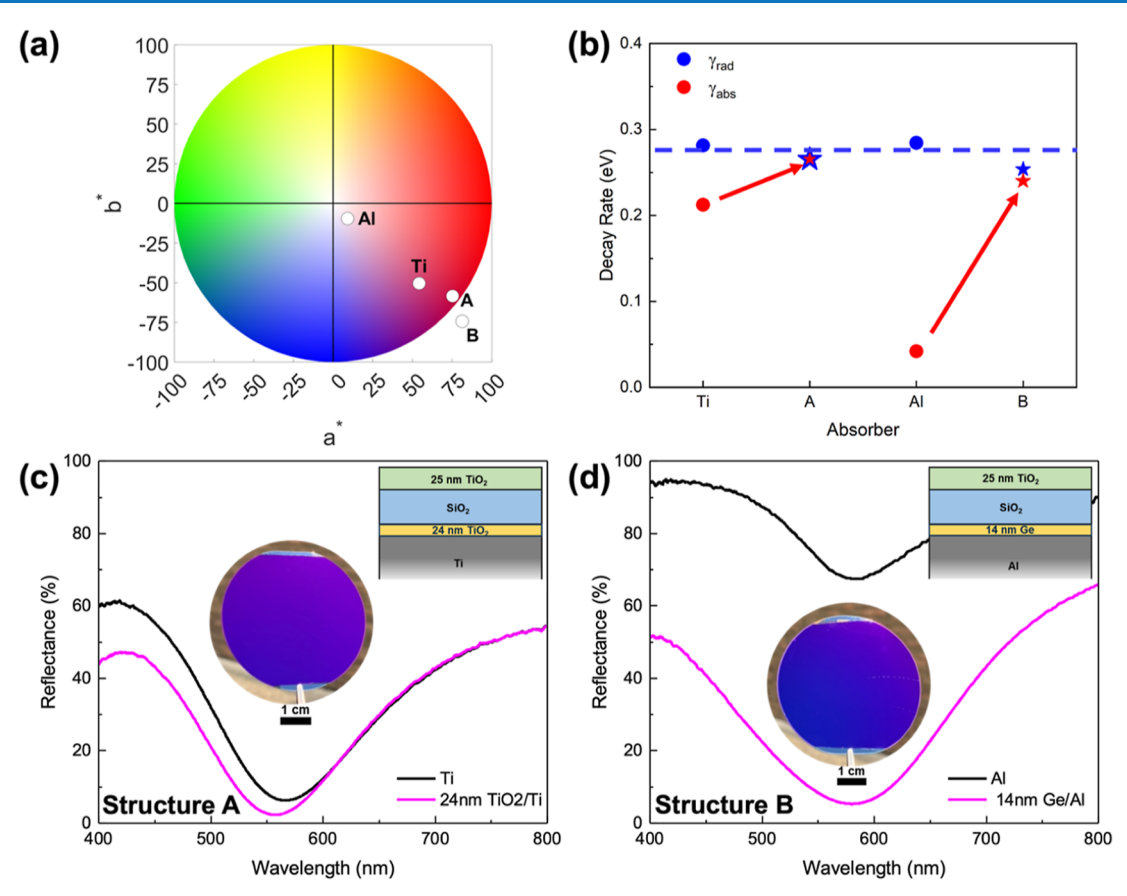


Figure 7. (a) CIEL*a*b* coordinates of structures A and B and their corresponding HLA structure calculated from TMM simulation. (b) Decay rate extracted using TCMT for structures in (a). (c) Experimentally recorded reflection spectra of structure A and its corresponding HLA. Inset: photo of fabricated structure A. (d) Experimentally recorded reflection spectra of structure B and its corresponding HLA. Inset: photo of fabricated structure B.

difference is observed across these samples with Si performing the best, while Al shows almost a neutral color. The recorded reflection spectra (Figure 5a) show a red shift in the resonance wavelength compared to the designed dark magenta color (Figure 4) due to a lack of deposition thickness control in the TiO₂ layer. Nevertheless, chromaticity (Figure 5b) and color appearance (Figure 5c) still match closely to what TCMT predicts.

Chromaticity of a Trilayer MDM Structural Color. Note that in the previous case of 25 nm TiO₂/SiO₂/absorber structure, the radiative loss is always larger than the absorption loss $(\gamma_{abs} > \gamma_{rad})$ for the absorber selected (Figure 4c), indicating that the system is always in an undercoupled regime due to the single lossy channel within the cavity. As a result, the produced color accidently resembles the trends of the absorber absorbance. To remedy this problem and also show that TCM is valid for other forms of trilayer structures, a metal/dialectic/metal (MDM) structure is considered in the form of 15 nm Ag/SiO₂/absorber, where both the top and bottom layers are responsible for the absorptive loss. Similar to the case of HLA, the SiO₂ layer in the MDM structure with different thicknesses is being calculated to achieve the same dark magenta color for various absorbing substrates (Figure 6a). The CIEL*a*b* diagram is being plotted for chroma comparison based on TMM simulation. In contrast to the HLA structure proposed before, the 15 nm Ag/SiO₂/absorber structure shows a very different trend (Figure 6b) in color chroma: the chromaticity order does not follow the decreasing order of absorber reflection as was the case for HLA where the structure with the Si substrate takes the lead. Instead, the structure with Pt shows the best chromaticity takes (except for the yellow color where gold has intrinsic broad-band absorption at shorter wavelengths). Further extraction of the decay rates (Figure 6c) reveals the underlying mechanism responsible for this change in trend. Once the top layer of the cavity has been changed from TiO2 to Ag, an increment in the absorption loss is observed due to the absorptive nature of silver as well as a decrease in the radiative loss with the electric field being more confined and enhanced (Figure S11) inside the SiO₂ layer (i.e., a better cavity quality). Therefore, the Ag/ SiO₂/absorber system can explore both the undercoupled regime $(\gamma_{abs} > \gamma_{rad})$ and the overcoupled regime $(\gamma_{rad} > \gamma_{abs})$ and even critical coupling when the two decay constant matches with each other.²⁷ High-loss absorbers such as Si, Ge, and Ti set the cavity under overcoupling, while low-loss absorbers like Al and Ag set the cavity under undercoupling. With moderate absorption near 550 nm, Cu and Pt push the cavity close to critical coupling and therefore give the best chroma performance. These trends are being fully captured by TCMT as shown in Figure 6d. Similar chromaticity performances are also observed in yellow, magenta, and cyan color by changing the SiO₂ layer thickness (Figures S8-S10 and S12). Another observation made out of the above HLA and MDM structure indicates that a wider color gamut can be achieved when a high chroma color can be achieved. As shown in Figures S13 and S14, a wider span in color space is observed

with Si or Pt in the 25 nm $TiO_2/SiO_2/absorber$ or the 15 nm $Ag/SiO_2/absorber$ structure when the SiO_2 thickness is swept from 0 to 400 nm with 5 nm interval.

Improving Color Chromaticity with TCM. The conclusions from TCM analysis can also help to address some challenges in structures that normally yield low color chroma. One such case is cavities with too high background reflection, which makes it very difficult to cause complete destructive interference with the reflected beam from the top surface. With the understanding that a matching of the two decay rates is required to yield high color chroma, an increment in the absorptive loss is desired with a highly reflective substrate (i.e. usualy comes with a very large n or κ). Considering the large imaginary part k of a typical high reflective substrate, an enhanced interfacial absorption can be made between a high refractive index dielectric and the substrate according to eq 5, where a smaller difference between n_0^2 and $n^2 + \kappa^2$ can be achieved. Hence, an ultrathin high refractive index material can be inserted between the SiO₂ layer and the absorber to improve its color chroma while minimizing any structural change to the stack. We will use a few examples to illustrate. In one example, a thin layer of lossless TiO2 is inserted between the SiO₂ and Ti layer, resulting in structure A (further details can be found in Figure S18). A TCM calculation indicates that the absorption loss is being increased (Figures 7b and S16) due to the addition of the high refractive index TiO₂ layer. As a result, an improvement in color can be clearly seen in Figure 7a (from a bare Ti substrate to structure A). In the second example, a thin Ge layer is added right on top of Al, giving structure B, i.e., 25 nm TiO₂/SiO₂/Ge/Al. As shown in Figure S17, with the increment in Ge thickness, a second dip with increasing resonance wavelength is observed, which corresponds to an extra resonance cavity within the Ge layer due to its high refractive index. This effect is related to the resonance effect formed within an ultrathin Ge layer on the metal surface due to the complex reflection coefficient contributing to a very large reflection phase 18,28 We choose 14 nm Ge as an add-on layer (25 nm TiO₂/SiO₂/14 nm Ge/Al) where resonance inside the Ge layer overlaps the resonance of the original HLA cavity and thus broadens the reflection dip. On the other hand, the lossy nature of Ge also boosts the absorption loss of the entire cavity (Figure 7b). As a result, the color chromaticity gets significantly improved as plotted in Figure 7a. The asfabricated samples based on structures A and B with dark magenta color are shown in Figure 7c,d inset along with the change in the reflection spectra compared to their original HLA design. The same strategy works for other colors in yellow, magenta, and cyan as well (Figures S15 and S16). It is worth noting that the extracted decay rates of structure B underestimate the broadening of the dip from the second resonance inside the Ge layer. This can be understood as the current TCM model only accounts for a single cavity with a single port where the absorption line shape is a Lorentzian function as expressed in eq 3. We also notice that the TCM captures the spectrum feature more accurately when the material dispersion is small near the resonant wavelength and could lead to larger deviation with an abrupt change in refractive index (e.g., Cu and Au). Further coupling between the cavities should be considered in structure B with a more complicated expression for the overall absorption of the structure, which is beyond the scope of this work.

CONCLUSIONS

In summary, a cavity-based temporal analysis is developed and applied to trilayer structures to gain insights into the color chroma behavior. The experimental results show that the TCM approach is very promising and general in predicting the chromaticity of the trilayer structure even without the inclusion of material dispersion. A high chromatic subtractive color can be achieved once the two decay channels $\gamma_{\rm abs}$ and $\gamma_{\rm rad}$ are balanced and maximized with the trilayer structural color. Both theoretical and experimental evidence support the prediction from TCM and provide a new design principle for high chromatic structural color production.

ASSOCIATED CONTENT

Solution Supporting Information

The Supporting Information is available free of charge at https://pubs.acs.org/doi/10.1021/acsphotonics.3c00481.

Optical properties of various absorbers; reflection spectra and temporal coupled analysis results of a 25 nm TiO₂/SiO₂/absorber structural color; reflection spectra and temporal coupled analysis results of a 15 nm Ag/SiO₂/absorber structural color; achievable color gamuts of a 25 nm TiO₂/SiO₂/absorber and a 15 nm Ag/SiO₂/absorber; and temporal coupled analysis results of structural colors with improved chromaticity (PDF)

AUTHOR INFORMATION

Corresponding Author

L. Jay Guo — Macromolecular Science and Engineering, University of Michigan, Ann Arbor, Michigan 48109, United States; Department of Electrical Engineering and Computer Science, University of Michigan, Ann Arbor, Michigan 48109, United States; orcid.org/0000-0002-0347-6309; Email: guo@umich.edu

Authors

Wei-Jie Feng — Macromolecular Science and Engineering, University of Michigan, Ann Arbor, Michigan 48109, United States; © orcid.org/0000-0002-5658-6595

Yian Cheng – Department of Electrical Engineering and Computer Science, University of Michigan, Ann Arbor, Michigan 48109, United States

Complete contact information is available at: https://pubs.acs.org/10.1021/acsphotonics.3c00481

Funding

The authors would like to thank the National Science Foundation (NSF PFI-008513) for the support of this work.

Notes

The authors declare the following competing financial interest(s): The work reported in this manuscript is the subject of a US provisional patent application.

REFERENCES

- (1) Fairchild, M. D. Color Appearance Models; Wiley, 2013.
- (2) Ji, C.; Lee, K.; Xu, T.; Zhou, J.; Park, H. J.; Guo, L. J. Engineering Light at the Nanoscale: Structural Color Filters and Broadband Perfect Absorbers. *Adv. Opt. Mater.* **2017**, *5*, 1700368.
- (3) Xuan, Z.; Li, J.; Liu, Q.; Yi, F.; Wang, S.; Lu, W. Artificial Structural Colors and Applications. *Innovation* **2021**, *2*, 100081.

- (4) Zhao, Y.; Zhao, Y.; Hu, S.; Lv, J.; Ying, Y.; Gervinskas, G.; Si, G. Artificial Structural Color Pixels: A Review. *Materials* **2017**, *10*, 944.
- (5) Song, M.; Feng, L.; Huo, P.; Liu, M.; Huang, C.; Yan, F.; Lu, Y. q.; Xu, T. Versatile full-colour nanopainting enabled by a pixelated plasmonic metasurface. *Nat. Nanotechnol.* **2023**, *18*, 71–78.
- (6) Bao, Y.; Yu, Y.; Xu, H.; Guo, C.; Li, J.; Sun, S.; Zhou, Z. K.; Qiu, C. W.; Wang, X. H. Full-colour nanoprint-hologram synchronous metasurface with arbitrary hue-saturation-brightness control. *Light Sci. Appl.* **2019**, *8*, 95.
- (7) Daqiqeh-Rezaei, S.; Dong, Z.; You En Chan, J.; Trisno, J.; Ng, R. J. H.; Ruan, Q.; Qiu, C. W.; Mortensen, N. A.; Yang, J. K. Nanophotonic Structural Colors. *ACS Photonics* **2020**, *8*, 18–33.
- (8) Shurvinton, R.; Lemarchand, F.; Moreau, A.; Lumeau, J. High-Chroma Color Coatings Based on Ag/SiO2/Ti/SiO2 Structures. *Adv. Photonics Res.* **2022**, *3*, 2200102.
- (9) Yang, Z.; Ji, C.; Liu, D.; Guo, L. J. Enhancing the Purity of Reflective Structural Colors with Ultrathin Bilayer Media as Effective Ideal Absorbers. *Adv. Opt. Mater.* **2019**, *7*, 1900739.
- (10) Yang, Z.; Ji, C.; Cui, Q.; Guo, L. J. High-Purity Hybrid Structural Colors by Enhancing Optical Absorption of Organic Dyes in Resonant Cavity. *Adv. Opt. Mater.* **2020**, *8*, 2000317.
- (11) Suh, W.; Wang, Z.; Fan, S. Temporal Coupled-Mode Theory and the Presence of Non-Orthogonal Modes in Lossless Multimode Cavities. *IEEE J. Quant. Electron.* **2004**, *40*, 1511–1518.
- (12) Fan, S.; Suh, W.; Joannopoulos, J. D. Temporal coupled-mode theory for the Fano resonance in optical resonators. *J. Opt. Soc. Am.* **2003**, *20*, 569.
- (13) Byrnes, S. J. Multilayer Optical Calculations. 2016, arXiv preprint arXiv:1603.02720.
- (14) Jung, I.; Kim, H.; Oh, S.; Kwak, H.; Ju, S.; Kim, M.; Jung, J. H.; Baac, H. W.; Ok, J. G.; Lee, K. T. Understanding a spectral response in a metal—dielectric—metal cavity structure: The role of constituent metals. *Opt Laser. Technol.* **2023**, *158*, 108772.
- (15) Yang, C.; Shen, W.; Zhang, Y.; Li, K.; Fang, X.; Zhang, X.; Liu, X. Compact Multilayer Film Structure for Angle Insensitive Color Filtering. *Sci. Rep.* **2015**, *5*, 9285.
- (16) Yang, C.; Ji, C.; Shen, W.; Lee, K. T.; Zhang, Y.; Liu, X.; Guo, L. J. Compact Multilayer Film Structures for Ultrabroadband, Omnidirectional, and Efficient Absorption. *ACS Photonics* **2016**, 3, 590–596.
- (17) Seo, M.; Kim, J.; Oh, H.; Kim, M.; Baek, I. U.; Choi, K.; Byun, J. Y.; Lee, M. Printing of Highly Vivid Structural Colors on Metal Substrates with a Metal-Dielectric Double Layer. *Adv. Opt. Mater.* **2019**, *7*, 1900196.
- (18) Kats, M. A.; Blanchard, R.; Genevet, P.; Capasso, F. Nanometre optical coatings based on strong interference effects in highly absorbing media. *Nat. Mater.* **2013**, *12*, 20–24.
- (19) Rahman, M. A.; Kim, D. K.; Lee, J.-K.; Byun, J. Y. To realize a variety of structural color adjustments via lossy-dielectric-based Fabry-Perot cavity structure. *Nanophotonics* **2022**, *11*, 4855–4868.
- (20) Cheng, F.; Gao, J.; Luk, T. S.; Yang, X. Structural color printing based on plasmonic metasurfaces of perfect light absorption. *Sci. Rep.* **2015**, *5*, 11045.
- (21) Lee, K.; Seo, S.; Guo, L. J. High-Color-Purity Subtractive Color Filters with a Wide Viewing Angle Based on Plasmonic Perfect Absorbers. *Adv. Opt. Mater.* **2015**, *3*, 347–352.
- (22) Park, C.-S.; Lee, S.-S. Vivid Coloration and Broadband Perfect Absorption Based on Asymmetric Fabry-Pérot Nanocavities Incorporating Platinum. ACS Appl. Nano Mater. 2021, 4, 4216–4225.
- (23) Ruan, Z.; Fan, S. Temporal Coupled-Mode Theory for Fano Resonance in Light Scattering by a Single Obstacle. *J. Phys. Chem. C* **2010**, *114*, 7324–7329.
- (24) Manceau, J.-M.; Zanotto, S.; Sagnes, I.; Beaudoin, G.; Colombelli, R. Optical critical coupling into highly confining metal-insulator-metal resonators. *Appl. Phys. Lett.* **2013**, *103*, 091110.
- (25) Park, G. C.; Park, K. Critically coupled Fabry—Perot cavity with high signal contrast for refractive index sensing. *Sci. Rep.* **2021**, *11*, 19575.

- (26) Ma, S.; Xiao, S.; Zhou, L. Resonant modes in metal/insulator/metal metamaterials: An analytical study on near-field couplings. *Phys. Rev. B* **2016**, 93, 045305.
- (27) Qu, C.; Ma, S.; Hao, J.; Qiu, M.; Li, X.; Xiao, S.; Miao, Z.; Dai, N.; He, Q.; Sun, S.; et al. Tailor the Functionalities of Metasurfaces Based on a Complete Phase Diagram. *Phys. Rev. Lett.* **2015**, *115*, 235503
- (28) Lee, K.; Seo, S.; Lee, J. Y.; Guo, L. J. Strong Resonance Effect in a Lossy Medium-Based Optical Cavity for Angle Robust Spectrum Filters. *Adv. Mater.* **2014**, *26*, 6324–6328.